Computational prediction of deformation behavior of TRIP steels under cyclic loading

Tomita, Yoshihiro

Iwamoto, Takeshi

(Citation)
International Journal of Mechanical Sciences,43(9):2017-2034

(Issue Date)
2001-09

(Resource Type)
journal article

(Version)
Accepted Manuscript

(URL)
https://hdl.handle.net/20.500.14094/90000022

Computational Prediction of Deformation Behavior of TRIP Steels under Cyclic Loading

Yoshihiro Tomita* and Takeshi Iwamoto**

*Graduate School of Science and Technology, Kobe University,
Rokkodai, Nada, Kobe 657-8501, JAPAN

**Faculty of Engineering, Hiroshima University,
Kagamiyama, Higashi-hiroshima, Hiroshima 739-8527, JAPAN

ABSTRACT

A constitutive equation accounting for strain rate, temperature and applied stress system dependencies of strain-induced martensitic transformation is given. A series of computational prediction of monotonic and cyclic deformation behavior including tension, compression and shearing of typical 304 austenitic stainless steel, have been performed under different environmental temperatures from 77K to 353K. The effect of stress range, pre-strain, temperature and applied stress system on such responses of TRIP steels as the evolution of martensitic phase, the accumulated plastic strain, and the asymptotic nature of the stress-strain relation with an increase in the number of cycles is clarified. The predictability of the present constitutive model is checked against the experimental results. Furthermore, simulation of the cyclic deformation behavior of TRIP steel bars with ringed notch is performed.

Corresponding address:
Yoshihiro TOMITA
Department of Mechanical Engineering
Faculty of Engineering, Kobe University
Nada, Kobe 657-8501, JAPAN
Tel: +81-78-803-6125
Fax: +81-78-803-6155
tomita@mech.kobe-u.ac.jp http://solid.mech.kobe-u.ac.jp

1. Introduction

Martensitic transformation of transformation-induced plasticity (TRIP) steel is observed during large deformation in the low-temperature range. A TRIP steel possesses advantageous mechanical properties including high strength, ductility and toughness due to the effect of strain-induced martensitic transformation which strongly depends on temperature, stress, strain and strain rate. Therefore, computational simulations using an appropriate constitutive equation are indispensable for predicting the deformation process as well as the final strength of the products. To date, the constitutive equation accounting for the temperature and strain effect on the martensitic transformation [1] and its generalization to account for the effect of stress state [2], strain rate [3] and stress state for stacking fault energy [4] have been proposed and computational simulations have been conducted to exemplify the transformation behavior and the mechanisms in order to improve the mechanical properties through the forming processes. However, the problems associated with the predictability of the constitutive equation for the cyclic deformation process are still unclear.

In order to clarify the validity of the constitutive equations, a series of computational simulation are carried out for cyclic loading under such different stress systems as tension, compression and shearing. Subsequently, computationally predicted results are compared with results [5],[6] obtained from carefully performed experiments which include the effect of stress range, number of cycles and pre-strains on the subsequent response of TRIP steels. A simple equation is proposed to reproduce the numerically predicted cyclic deformation behavior. Furthermore, the computational method thus established is applied to the prediction of the deformation behavior of ringed-notched bars deformed under cyclic loading.

2. Constitutive Equation

Olson and Cohen [1] established a model for strain-induced martensitic transformation kinetics, which can express the temperature dependence of the transformation phenomena. This phenomenological model was constructed under the assumption that the transformation occurred at the intersection of the shear band in the austenite mother phase with a certain probability. Stringfellow et al. [2] generalized the Olson and Cohen model so as to include the stress state and the contribution of the martensite phase to the strength. Tomita and Iwamoto [3] modified the two models to account for the experimental finding that the mode of the deformation behavior is controlled by the shear band mode as the strain rate increases [7]. The rate of increase of the volume fraction of martensite, $\dot{f}^{\alpha'}$, is given by

$$\dot{f}^{\alpha'} = (1 - f^{\alpha'})(A\dot{\bar{\varepsilon}}_{\gamma}^{pslip} + B\dot{g}), \tag{1}$$

$$A = \alpha p n \eta \left(f^{sb}\right)^{n-1}\left(1 - f^{sb}\right), \quad B = \eta \frac{dp}{dg}(f^{sb})^{n} H(\dot{g}),$$

where $\dot{\bar{\varepsilon}}_{\gamma}^{pslip}$ is the equivalent strain rate of slip deformation in austenite, f^{sb} is the volume fraction of the shear band, p is the probability that an intersection forms a martensitic embryo [2],[3], g is the driving force for martensitic transformation, $H(\dot{g})$ is the Heaviside step function with respect to $\dot{g}$ which describes the irreversible process of martensitic transformation, and n and η are geometric constants. α is a parameter related to the stacking fault energy and is a function of temperature T [1], strain rate $\dot{\bar{\varepsilon}}_{\gamma}^{pslip}$ [3] and the stress triaxiality parameter $\Sigma = \sigma_{ii} / \left(3\bar{\sigma}\right)$ [4] as

$$\alpha = \left(\alpha_1 T^2 + \alpha_2 T + \alpha_3 - \alpha_4 \Sigma\right)\left(\frac{\dot{\bar{\varepsilon}}_{\gamma}^{pslip}}{\dot{\varepsilon}_y}\right)^{M}, \tag{2}$$

where M is the strain rate sensitivity exponent, $\alpha_1 - \alpha_4$ are material parameters and $\dot{\varepsilon}_y$ is the reference strain rate.

For the loading function, to account for the experimentally observed evidence [4] that uniaxial tension and compression curves for austenite and martensitic phase in TRIP steels are different, the third invariant of deviatoric stress σ'_{ij} is introduced as

$$f\left(J_2, J_3\right) = J_2 - \kappa \frac{J_3}{J_2^{1/2}} - \frac{1}{3}\bar{\sigma}^2 = 0 \tag{3}$$

$$J_2 = \frac{1}{2}\sigma'_{ij}\,\sigma'_{ij}, \quad J_3 = det\left|\sigma'_{ij}\right|, \quad \bar{\sigma} = \sqrt{3\left(J_2 - \kappa \frac{J_3}{J_2^{1/2}}\right)}$$

where $\bar{\sigma}$ is the equivalent stress and κ is the parameter which reflects the development of microstructure and texture inside the materials. The simplified evolution equation for κ proposed by Miller and McDowell [8] is

$$\dot{\kappa} = C_{\kappa}\left(1 - \kappa\right)\dot{\bar{\varepsilon}}^{pslip} \tag{4}$$

where C_{κ} is a constant.

Next, using the standard notation of an updated Lagrangian formulation [9],[10], the total strain rate $\dot{\varepsilon}_{ij}$ is the rate of stretching tensor and is assumed to be the sum of the elastic component $\dot{\varepsilon}_{ij}^{e}$ and the plastic component $\dot{\varepsilon}_{ij}^{p}$. The plastic strain rate $\dot{\varepsilon}_{ij}^{p}$ is decomposed into the plastic strain rate $\dot{\varepsilon}_{ij}^{pslip}$ induced by slip deformation in austenite and martensite, and $\dot{\varepsilon}_{ij}^{ptrans}$ induced by the transformation. Furthermore, the transformation plastic strain rate is split

into a deviatoric part, $\dot{\varepsilon}_{ij}^{pshape}$, related to shape change, and a dilatational part, $\dot{\varepsilon}_{ij}^{pdilat}$, expressing volume change. Under the assumptions that the strain rate $\dot{\varepsilon}_{ij}^{pshape}$ is considered to be coaxial with deviatoric stress [2] and that $\dot{\varepsilon}_{ij}^{pdilat}$ can be expressed in terms of volume change Δv, which has a value of $0.02-0.05$ for austenite steel, the plastic strain rate $\dot{\varepsilon}_{ij}^{p}$ can be expressed as

$$\dot{\varepsilon}_{ij}^{p} = p_{ij}\dot{\bar{\varepsilon}}^{p} + s_{ij}\Delta v\dot{f}^{\alpha'}$$

$$p_{ij} = \frac{3}{2\bar{\sigma}}\frac{\partial f}{\partial \sigma_{ij}}, \quad s_{ij} = -p_{ij}\Sigma + \frac{\delta_{ij}}{3} \tag{5}$$

$$\dot{\bar{\varepsilon}}^{p} = \dot{\bar{\varepsilon}}^{pslip} + R\dot{f}^{\alpha'} + \Sigma\Delta v\dot{f}^{\alpha'},$$

where $\dot{\bar{\varepsilon}}^{p}$ is the work equivalent measure of the equivalent plastic strain rate with respect to equivalent stress $\bar{\sigma}$ defined by Eq.(3) and R is the parameter accounting for the magnitude of shape changes and depends on the stress [2]. The constitutive equation for the stress rate can be established by introducing the plastic strain rate in Eq.(3) into the thermo-elastic constitutive equation, as discussed by Tomita et al. [11]

$$\overset{\nabla}{S}_{ij} = D_{ijkl}^{e}(\dot{\varepsilon}_{ij} - \dot{\varepsilon}_{ij}^{p}) - \beta_{ij}\dot{T} \tag{6}$$

$$\beta_{ij} = \frac{\alpha_E}{1-2\nu}\delta_{ij} - \frac{1}{E}\frac{\partial E}{\partial T}\sigma_{ij},$$

where $\overset{\nabla}{S}_{ij}$ is the Jaumann rate of the Kirchhoff stress S_{ij} which is identical to the Cauchy stress σ_{ij} in the current state, D_{ijkl}^{e} is the elastic stiffness tensor which contains the elasticity modulus E and Poisson's ratio ν. α_E is the thermal expansion coefficient.

The constitutive equation for a two-phase composite material of austenite with the volume fraction of the martensitic phase $f^{\alpha'}$ is established in a manner similar to that described by Stringfellow et al. [2], applying Eshelby's theory [12]. The forward gradient method is introduced to improve computational efficiency.

The constitutive parameters employed are those indicated in previous works [4],[13] and the parameters κ and C_κ in Eq.(3) are newly determined based on the experimental results [4]. For the remaining material parameters required for the developed constitutive equation, a similar procedure [2],[3] is applied to experimentally obtained data, as indicated in the Appendix.

3. Boundary Value Problem and Computational Method

With an updated Lagrangian formulation, the weak form of the equation governing the rate of stress and traction yields the virtual work principle [14],[15],

$$\int_V \left(\dot{S}_{ij} + \sigma_{lj} v_{i,l}\right)\delta v_{i,j} dV = \int_{S_t} \dot{P}_i \delta v_i dS \,, \tag{7}$$

where $\dot{P}_i$ is the nominal traction rate and δv_i is the virtual velocity satisfying the homogeneous boundary condition over surface S_v.

The numerical procedure uses the finite element method [10],[11] developed based on the virtual work principle (7) along with the proposed constitutive equations (5) and (6).

For homogeneous deformation, a single finite element is employed and the velocity boundary conditions corresponding to the specific strain rate are specified for the nodal velocity of the finite element. Figure 1 shows the computational model for the ringed notch specimen. Due to symmetric deformation, the deformation behavior has been simulated with the finite element discretization shown in the figure. Each quadrilateral consists of four crossed-triangular axisymmetric elements.

4. Results & Discussion

4.1 Monotonic Tension and Compression

Figure 2 shows the predicted (a) stress-strain relations and (b) volume fraction of martensitic phase by thus-obtained material parameters and these experimentally obtained results [4]. The corresponding reproduction of the stress-strain relation and the evolution of volume fraction of martensitic phase shown in Fig.2 is quite good. For comparison, evaluation of the stress-strain relation for different stress conditions was performed under an environmental temperature of 77K. Fig.3 shows the predicted (a) stress-strain relation and (b) volume fraction of martensitic phase with respect to equivalent plastic strain for tension, compression and shear deformation under relatively small strain of which magnitude is comparable to the case of cyclic loading that will be discussed in the following section. The results clearly capture the stress state dependency of the evolution of the martensitic phase, which results in the difference in the magnitude of deformation resistance of the materials. These tendencies well correspond to the experimentally obtained results [5]. However, quantitative comparison is required for further identification of the material constants introduced in the present constitutive equation.

4.2 Effect of stress system applied to cyclic uniform deformation

The computational simulation of plane strain block deformed under cyclic loading

with and without pre-strain at environmental temperatures of 77K and 298K was performed. The temperature of 77K corresponds to the lowest temperature achieved by cooling with liquid nitrogen with the maximum volume fraction of the martensitic phase, and 298K is for the case with maximum ductility [3] in our experiments. Three different strain ranges, 0.02, 0.03 and 0.04, were selected for the simulation.

In order to explain the characteristic feature of the deformation processes under cyclic loading condition, the typical cyclic stress-strain relation [6] is shown in Fig.4. In the figure, $\Delta\sigma$ is the stress range corresponding to the strain range $\Delta\varepsilon$, σ^{+}_{max} and σ^{-}_{max} are the absolute maximum values of stress attained during a deformation cycle, ΔS_i^P is the magnitude of strain difference at zero stress as indicated in the figure, e and S^p is the accumulation of the strain difference up to the Nth cycle. These notations will be used for the explanation of the cyclic deformation behavior under different loading conditions.

Figure 5 shows the stress-strain relations under (a) axial and (b) shear cyclic stress at 77K and 298K with a strain range $\Delta\varepsilon$=0.02. Due to the martensitic transformation, rapid hardening, which causes an increase in the stress range $\Delta\sigma$, and monotonic decrease in the width of the hysteresis loop ΔS_i^p with respect to strain, are observed. Eventually elastic cyclic loading can be approached in the case of low temperature, whereas plastic deformation remains in the case of high temperature and the deformation is mainly consumed in the austenitic phase. Figure 6 indicates the volume fraction of the martensitic phase $f^{\alpha'}$ and the stress range $\Delta\sigma$ with respect to the applied number of cycles N under (a) axial and (b) shear loading with strain range $\Delta\varepsilon$ = 0.02，0.03，0.04 and temperatures 77 and 298K. As expected, a rapid saturation of the volume fraction of the martensitic phase is attained with a larger strain range $\Delta\varepsilon$ at a lower temperature, which is manifested as the saturation of the stress range $\Delta\sigma$ at a lower number of cycles. On the other hand, the saturation of the stress range $\Delta\sigma$ was not observed at 40 cycles of loading in the high temperature range. The results obtained are similar to those experimentally obtained for type 304 austenitic stainless steel [6],[16]. It should be noted that the saturation value of the volume fraction of the martensitic phase for cyclic axial loading is higher than that for monotonic tension [13],[17], which is attributable to the different probability of martensitic transformation at the intersection of shear bands, as indicated in Eq.(1). That is, in cyclic loading, the transformation favorably occurs during the compression process. The stress-dependent features of cyclic deformation processes can be seen in Figs.5 (a) and (b), $\sigma^{+}_{\max} \geq \sigma^{-}_{\max}$, which are also attributable to the dependence of martensitic transformation on the stress as shown in Eq.(2). Thus, the typical nature of the cyclic deformation processes observed in TRIP steels is

attributable to the martensitic transformation due to plastic deformation.

4.3 Effect of pre-strain on cyclic deformation

Figure 7 shows stress-strain relations for (a) axial and (b) shear cyclic deformation with strain range $\Delta\varepsilon = 0.02$ and pre-strain $\varepsilon_{pre} = 0.02$ under environmental temperature 77K. Similar to the asymptotic nature observed in Fig.5 for the case without pre-strain, a gradual reduction of the width of stress-strain relation ΔS_i^p, an increase in stress range $\Delta\sigma$, and their saturation with the number of cycles are seen. The stress range $\Delta\sigma$ for shear deformation is larger than that for axial deformation. These characteristic features are compatible with those obtained from experiments [6].

The effect of pre-strain on the stress range and volume fraction of martensitic phase with respect to accumulated plastic strain can be seen in Fig.8. The asymptotic nature of cyclic stress-strain relations in Fig.7 implies that the rate of accumulation of plastic strain decreases as the number of cycles increases and asymptotically approaches a specific value, which is due to the martensitic transformation of the austenitic phase and is attributable to the identical saturation value of the martensitic phase for the case with different pre-strains, as shown in Fig. 8(b). On the other hand, the stress range $\Delta\sigma$ in Fig.8(a) increases with accumulated plastic strain S^p, whereas the rate of increase is suppressed with pre-strain ε_{pre}. This can be explained by the fact that the fraction of hardening due to martensitic transformation after pre-straining decreases as the magnitude of pre-strain increases.

4.4 Prediction of deformation behavior of TRIP steels under cyclic loading by simple equations

Based on a comprehensive experiment [16], the relation between stress range $\Delta\sigma$ and accumulated plastic strain S^p is established and expressed as

$$\Delta\sigma = (\sigma_S - \sigma_0)\{1 - \exp[-a(S^p)^i]\} + \sigma_0 \tag{8}$$

where σ_S is the saturation value of stress range with increasing accumulated plastic strain, σ_0 is the initial value of stress range for N = 0, a is a material constant. To reproduce the experimentally obtained results which exhibit substantial temperature dependence a parameter i takes a value of 2 in the case of low environmental temperature and 1 in the case of room and high temperature.

With regard to the relationship between volume fraction of martensitic phase and accumulated plastic strain as shown in Fig.8(b), the martensitic phase gradually starts to increase depending on the temperature and eventually saturates with the increase in accumulated plastic strain and exhibits an S-shaped curve. This phenomenon resembles the volume fraction of martensitic phase-plastic strain relations for monotonic loading so that in

order to approximately predict the martensitic transformation behavior for cyclic deformation process, the relation proposed by Olson and Cohen [1] for monotonic loading is extended to the case of cyclic loading and expressed as

$$f^{\alpha'} = 1 - \exp\{\beta_c[1 - \exp(-\alpha_c S^p)]^{n_c}\} + f_0^{\alpha'}, \quad (9)$$

where $f_0^{\alpha'}$ is the volume fraction of martensic phase at cycle number N = 0, and α_c, β_c, n_c are constants which are identified so as to reproduce the results.

Here, Eqs. (8) and (9) are applied to the prediction of stress range $\Delta\sigma$ and volume fraction of martensitic phase $f^{\alpha'}$ in relation to accumulated plastic strain S^p under different environmental temperatures. Fig. 9 shows (a) stress range $\Delta\sigma$-accumulated plastic strain S^p relation and (b) volume fraction of martensitic phase $f^{\alpha'}$-accumulated plastic strain S^p relation for axial cyclic deformation under $\Delta\varepsilon$ = 0.02. This figure indicates the capability of Eqs. (8) and (9) for reproducing the computationally estimated results with suitably identified parameters.

Figure 10 shows the variation of identified values of parameters (a) α_c and (b) β_c by the least mean squares method. α_c and β_c decrease with increasing of environmental temperature. The value α_c for shear deformation is larger than that for axial deformation in the low temperature range, whereas the relation becomes the reverse as the temperature increases. Furthermore, the value β_c for shear deformation is small as compared with that for axial deformation over the entire temperature range. As in the case of monotonic loading, parameters α_c and β_c that are expressed by the suitable function of temperature and deformation state may well predict the transformation process under cyclic loadings with different environmental conditions.

4.5 Cyclic deformation behavior of ringed notched specimen

Although quantitative comparison between computationally predicted results and those obtained experimentally was restricted to the case of monotonic deformation [13],[17],[18], based on the discussion in this section, we expect that the present computational strategy to predict the deformation behavior of TRIP steels will provide a valuable tool for clarifying the general feature of deformation under the monotonic, as well as the cyclic, loading process of TRIP steels. Here we consider the cyclic loading process of ringed-notched specimens at an environmental temperature of 77K.

The computational model employed is shown in Fig.3. The typical load-displacement relation for 40 continuous cycles is shown in Fig.11 (a). The corresponding load amplitude versus number of cycles is shown in (b). For comparison, nontransforming austenitic case is also shown. Since the deformation is localized to the notched region, the saturation of the

volume fraction of the martensitic phase is restricted to a rather small area. Therefore, the asymptotic nature of the load amplitude versus number of cycles can be seen in the early stage of the cycles, and the hysteresis loop in load-displacement relations is very small and converges very rapidly to the quasi-elastic deformation process. This also results in the small difference between the results for TRIP steels and nontransforming austenitic steel.

Figure 12(a) shows the evolution of the volume fraction of the martensitic phase for different numbers of cycles. The area with a high volume fraction of the martensitic phase starts from the notch root and penetrates into the interior of the specimen at approximately 45 degrees with respect to the tension axis. This martensitic transformation causes the distribution effect of the deformed region, as indicated in Fig.12(b) which shows the distribution of the equivalent plastic strain. The comparison between the evolution of plastic strain (b) for TRIP steels and (c) for the nontransforming austenitic steel, namely, the austenite phase, clearly exhibits the distribution effect. For comparison, Fig. 13 shows (a) equivalent plastic strain, (b) volume fraction of the martensitic phase and (c) axial stress distribution for monotonic tension and compression. Due to the high value of the transforming probability of the intersection site of micro shear bands to a martensitic embryo, the transformation in the case of compression is promoted further than that in the case of tension. Therefore, the evolution of the volume fraction of the martensitic phase under the cyclic loading process is mainly promoted during the compressive loading process. Furthermore, the blunting of the notch root proceeds in the order of tension, cyclic loading and compression, so that the volume fraction of the martensitic phase becomes saturated in the reverse order. For cyclic loading, further transformation mainly occurs in the austenitic phase during the compressive process.

5. Conclusions

In this study, the constitutive equation that models for martensitic transformation depending on strain rate, temperature and applied stress system, was developed as an extension of those proposed in [1] and [2]. The computational strategy for the prediction of the deformation behavior of TRIP steels was developed using the established constitutive equation. Subsequently, the computational strategy was applied to clarify the deformation behavior of cyclic axial tension and compression and shear deformation of TRIP steels with and without pre-strain ε_{pre}. The effect of stress $\Delta\sigma$ and strain $\Delta\varepsilon$ range, temperature T and pre-strain ε_{pre} on the stress-strain relation and the saturation nature of stress range $\Delta\sigma$ and strain range $\Delta\varepsilon$ in stress-strain relation were clarified. Due to the lack of information

of the materials employed in the experiments of cyclic loading, the discussion was restricted to a qualitative one; nevertheless, it was confirmed that the essential features of the deformation behaviors could be reproduced by the computational simulation. Based on thus-obtained computational results, the simple equation that reproduces the volume fraction of martensitic phase $f^{\alpha'}$ and the accumulated plastic strain S^p for cyclic loading process was established.

Finally, the computational simulation of the deformation behavior of TRIP steel bars with the ringed notch under uniaxial tension at 77K was performed. Since the predictability of the cyclic deformation behavior of TRIP steels for simple stress cases was verified by the present investigation, the deformation behavior thus predicted for the ringed-notched specimen under cyclic loading would provid suitable information of the deformation behavior of TRIP steels under complex loading.

Acknowledgements

Financial support from the Ministry of Education of Japan is gratefully acknowledged.

Appendix

Material parameters at temperature T employed in the present investigation are summarized. A discussion on the identification of material parameters is given in [2]-[4] .

Stress-strain relation for austenite and martensite phases is

$$\overline{\sigma} = \sigma_y + c_1\left\{1.0 - \exp\left(-c_2\overline{\varepsilon}_p\right)\right\}^{c_3}, \sigma_y = c_4\exp\left(-c_5 T\right),$$

where $c_1 = 1861.0$, $c_2 = 0.628$, $c_3 = 0.748$, $c_4 = 660.0$, $c_5 = 0.0027$ with elastic modulus $E_a = 215.7 - 0.0692T(GPa)$ and Poisson's ratio $\upsilon = 0.3$ for austenite phase and $c_1 = 1191.0$, $c_2 = 1.33$, $c_3 = 0.540$, $c_4 = 1056.0$, $c_5 = 0.0013$ with elastic modulus $E_m = 237.3 - 0.0692T(GPa)$ and Poisson's ratio $\upsilon = 0.3$ for martensite phase.

Evolution of volume fraction of martensitic phase is indicated as Eqs. (1) and (2) with material parameters $\eta = 4.5$, $M = 0.013$, $\alpha_1 = -2.02\times10^{-4}$, $\alpha_2 = 3.27\times10^{-2}$, $\alpha_3 = 11.7$, $\alpha_4 = 10.23$ for $T \le 273K$ and $\alpha_1 = 0.0$, $\alpha_2 = -7.92\times10^{-2}$, $\alpha_3 = 27.1$, $\alpha_4 = 10.23$ for $T \ge 273K$. The standard deviation σ_g, mean value g_0 and constant g_1 are 17.0, –276.0 and 28.7, respectively [2]-[4].

Constitutive equation for plastic strain rate is expressed as in Eq. (5) with $R_0 = 0.02$, $R_1 = 0.02$ and $\Delta v = 0.02$. Evolution equation for parameter κ is given by Eq.(3) with $C_k = 0.49$.

References

1. Olson GB, Cohen M. Kinematics of strain-induced martensitic nucleation. Metall Trans. A 1975: 6: 791 - 795.
2. Stringfellow RG, Parks DM, Olson GB. A constitutive model for transformation plasticity accompanying strain-induced martensitic transformation in metastable austenitic steels. Acta Metall. 1992: 40: 1703 - 1716.
3. Tomita Y, Iwamoto T. Constitutive modeling of TRIP steel and its application to the improvement of mechanical properties. Int. J. Mech. Sci. 1995: 37(12): 1295 – 1305.
4. Iwamoto T, Tsuta T, Tomita Y. Investigation on deformation mode dependence of strain-induced martensitic transformation in TRIP steels and modeling of transformation kinetics. Int. J. Mech. Sci. 1998: 40(2/3): 173 - 182.
5. Tanaka N, Shirasawa Y, Niitsu Y, Ikegami K. Experimental investigation of plastic deformation of SUS304 stainless steel at 77K, Trans. JSME Ser. A 1991: 57(543): 2775 - 2781. (in Japanese)
6. Yokotsuka T, Ikegami K. Cyclic plastic deformation at low temperature in liquid nitrogen and room temperature subsequent to pre – strain at low temperature in liquid nitrogen and room temperature. J. Soc. Mat. Sci., Japan 1999: 48(1): 38 – 43. (in Japanese)
7. Hecker SS, Stout MG, Staudhammer KP, Smith JL. Effect of strain state and strain rate on deformation induced transformation in 304 stainless steel: part I. magnetic measurements and mechanical behavior. Metall. Trans. A 1982: 13: 619 – 626.
8. Miller MP, McDowell DL. Modeling large strain multiaxial effects in FCC polycrystals. Int. J. Plast. 1996: 12 (7): 875 – 902.
9. Tomita Y, Shindo A, Kitagawa H. Bifurcation and post bifurcation behaviour of internally pressurized elastic-plastic circular tubes under plane strain conditions. Int. J. Mech. Sci. 1981: 23: 723 - 732.
10. Tomita Y. , Simulations of Plastic Instabilities in Solid Mechanics, Applied Mechanics Reviews 47-6, Part 1 (1994-6) 171-205
11. Tomita Y, Shindo A, Sasayama S. Plane strain tension of thermo-elasto-viscoplastic blocks. Int. J. Mech. Sci. 1990: 32: 613 - 622.
12. Eshelby JD. The determination of the elastic field of an ellipsoidal inclusion, and related problems. Proc. Roy. Soc. Lond., 1957: A241: 376 - 396.
13. Tomita Y, Shibutani Y. Estimation of deformation behavior of TRIP steels — smooth/ringed-notched specimens under monotonic and cyclic loading. Int. J. Plasticity, 2000: 16: 769 - 789.

14. Hill R. A general theory and uniqueness and stability in elastic-plastic solids. J. Mech. Phys. Solids 1958: 8: 236 - 249.
15. Kitagawa H, Seguchi Y, Tomita Y. An incremental theory of large strain and large displacement problems and its finite element application. Ing. Arch. 1972: 41: 213 - 224.
16. Shirasawa Y, Ikegami K, Niitsu Y. Experimental investigation of cyclic plastic deformation of stainless steel 304 at low temperature. Trans. JSME. Ser. A 1993: 59(566): 2427 – 2434. (in Japanese)
17. Tomita Y, Shibutani Y. Estimation and prediction of local strain-induced martensitic transformation. Arc. Mech. 1999: 51: 865 - 884.
18. Ogawa T, Taniyama A, Tomita Y, Shibutani Y, and Adachi, T. Local deformation behavior around ringed notch in TRIP steel bars under tension Proc. AEPA' 96 Advances in Engineering Plasticity and Its Applications 1996: 599-603, Elsevier Sci. Pub.

Figure captions

Fig. 1 Computational model of ringed notch specimen for finite element simulation.

Fig. 2 Predicted and experimentally obtained results for uniaxial tension and compression Solid lines and dotted lines are predicted results and □■○…are experimentally obtained results.

Fig. 3 Effect of stress system applied on the stress-strain relation and evolution of volume fraction of martensitic phase.

Fig. 4 Schematic illustration of cyclic stress – strain curve and explanation of stress range and accumulated plastic strain.

Fig. 5 Cyclic stress-strain curve under (a) axial stress and (b) shear stress at 77K and 298K with a strain range of 0.02.

Fig. 6 Volume fraction of the martensite and the stress range with respect to the applied number of cycles under (a) axial stress and (b) shear stress at 77K and 298K with strain range $\Delta\varepsilon$ = 0.02, 0.03 and 0.04.

Fig. 7 Cyclic stress – strain relations for (a) axial stress and (b) shear stress at 77K with pre-strain ε_{pre} =0.02 and strain range $\Delta\varepsilon$ =0.02.

Fig. 8 (a) Stress range – accumulated plastic strain and (b) volume fraction of martensite-accumulated plastic strain relations for various pre – strains at 77 K under axial cyclic loading.

Fig. 9 (a) Stress range and (b) volume fraction of martensite-accumulated plastic strain relations at various environmental temperatures for $\Delta\varepsilon$ = 0.02.

Fig. 10 Parameter α_c and β_c in Eq. (9) versus environmental temperature for $\Delta\varepsilon$ =0.02 under axial and shear cyclic loading.

Fig. 11 (a) Load-displacement relation and (b) load amplitude-number of cycle relation for ringed notched specimen under cyclic loading.

Fig. 12 Evolution of volume fraction of martensitic phase (a) for different number of cycles, equivalent plastic strain distribution for (b) TRIP steels and (c) nontransforming austenitic steel.

Fig. 13 Deformation behavior of ringed-notched specimen under monotonic tension and compression.

Figure 1

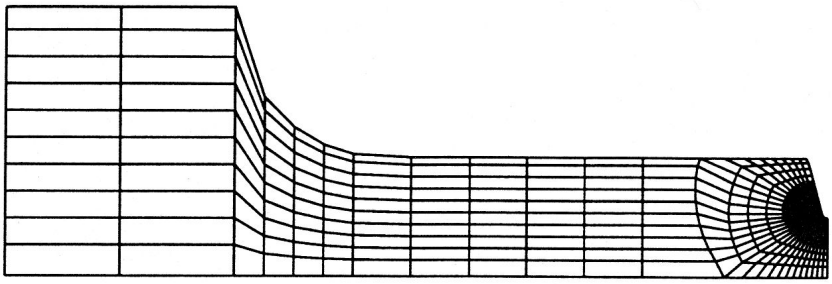

Computational Model

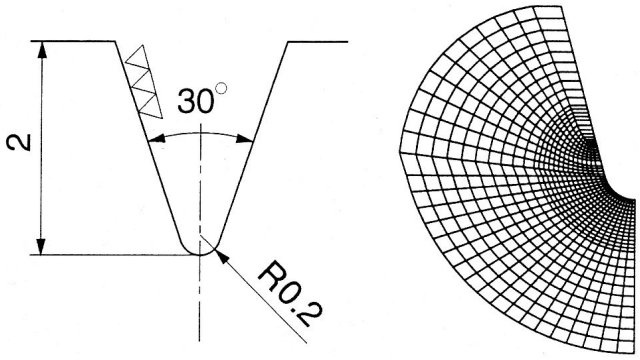

Magnification of Notch Root

Figure 2

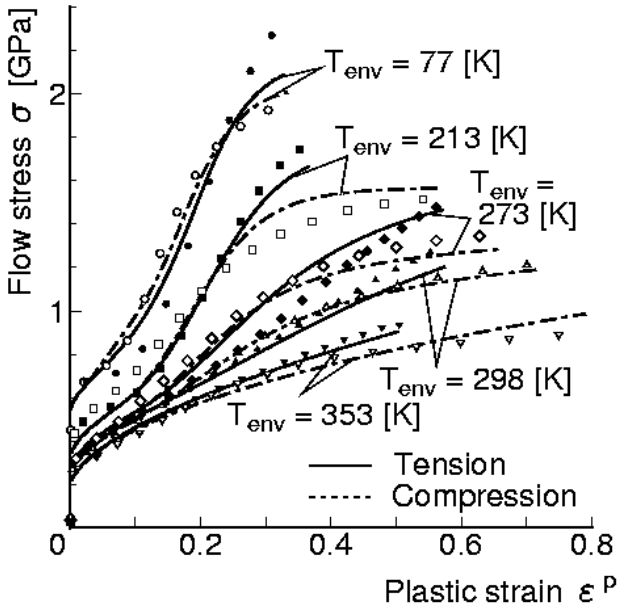

(a) stress – strain relation

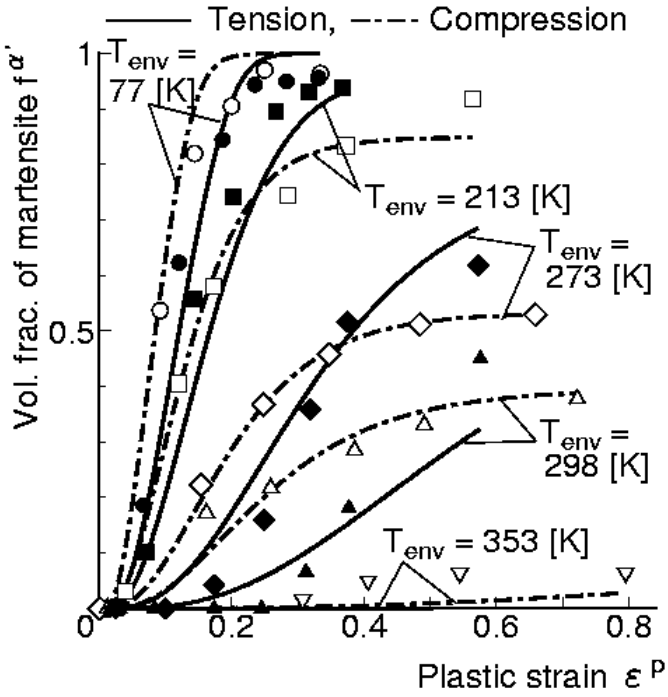

(b) volume fraction of martensitic phase-strain relation

Figure 3

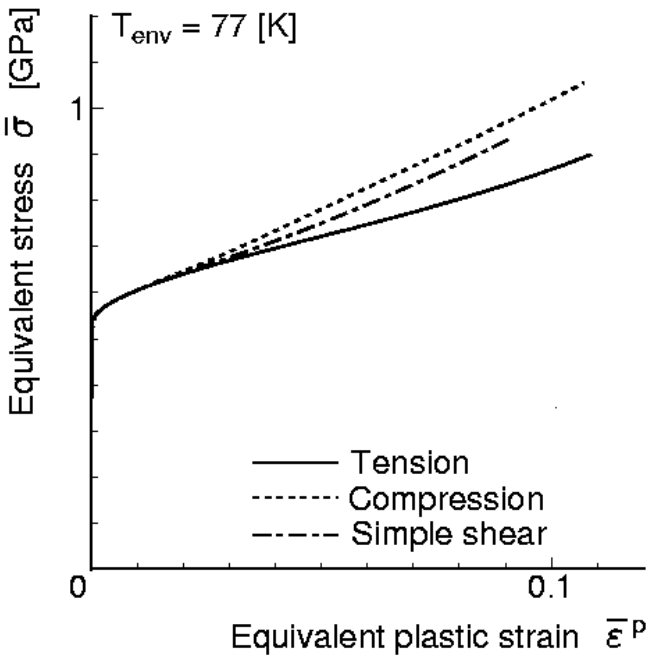

(a) Stress-strain relation

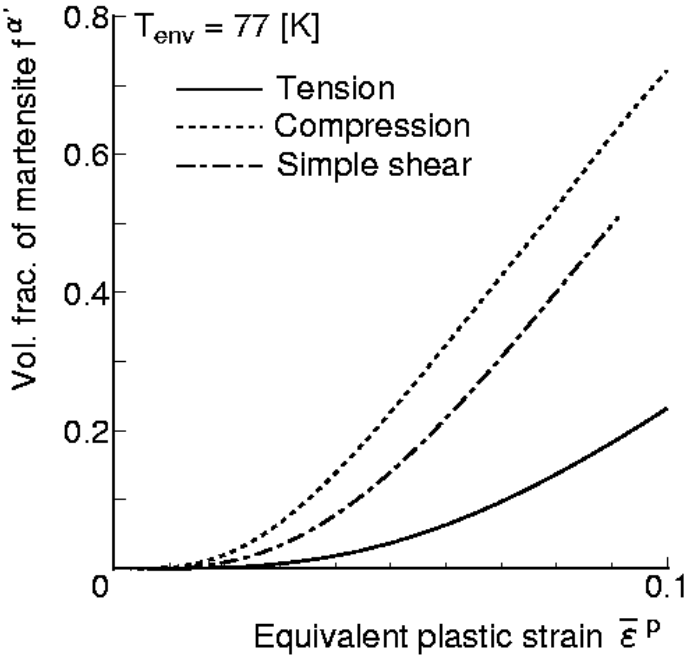

(b)Volume fraction of martensitic phase-strain relation

Figure 4

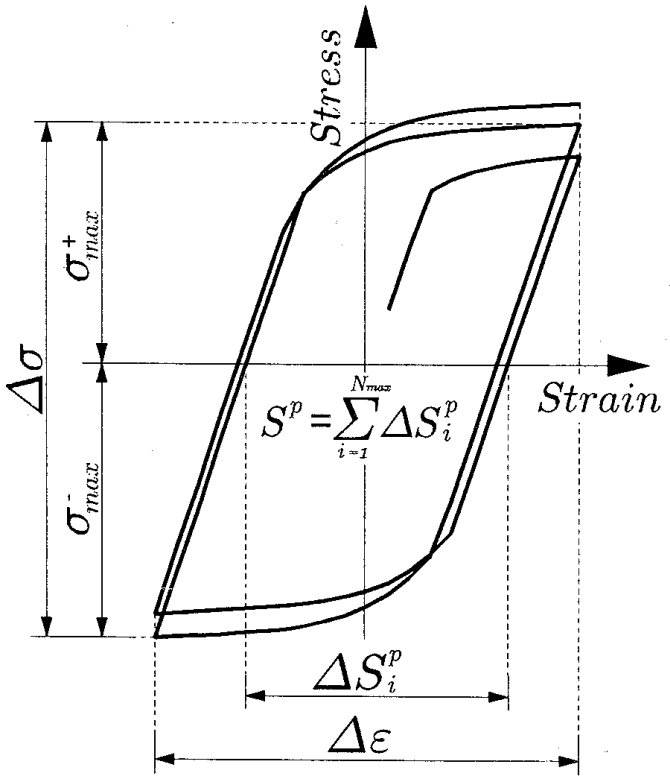
Stress
Strain
$\Delta\sigma$
σ^+_{max}
σ^-_{max}
$S^p = \sum_{i=1}^{N_{max}} \Delta S_i^p$
ΔS_i^p
$\Delta\varepsilon$

Figure 5

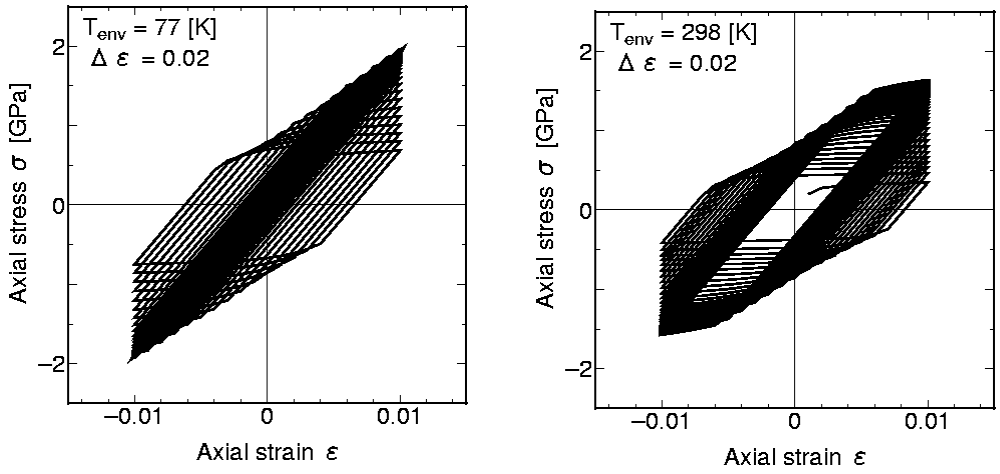

(a) axial stress

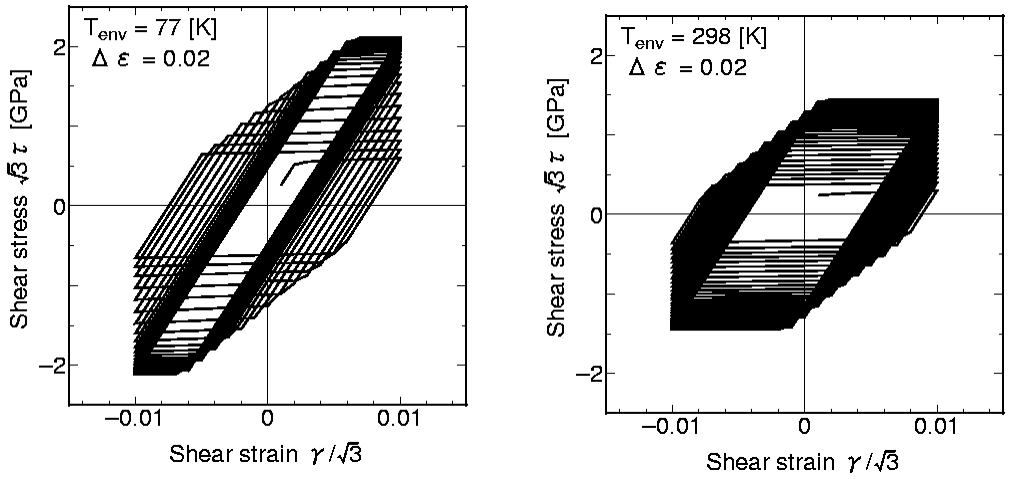

(b) shear stress

Figure 6

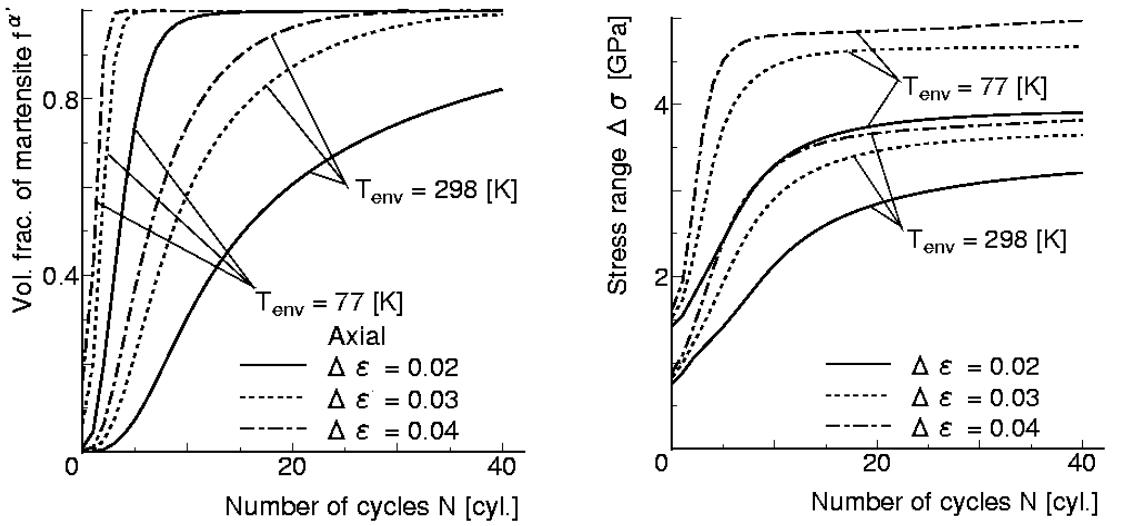

(a) axial stress

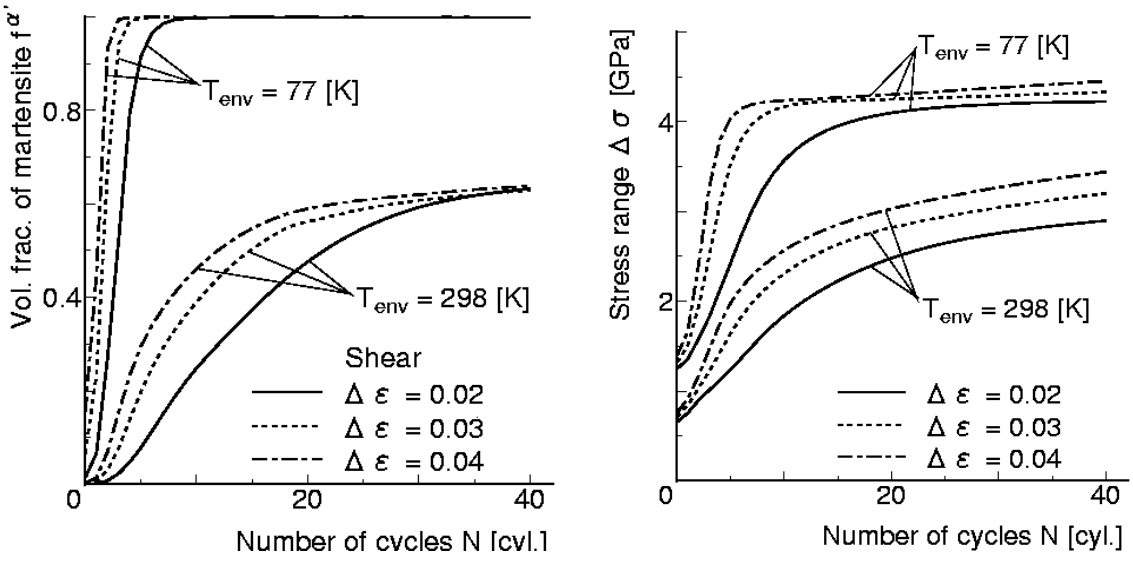

(b) shear stress

Figure 7

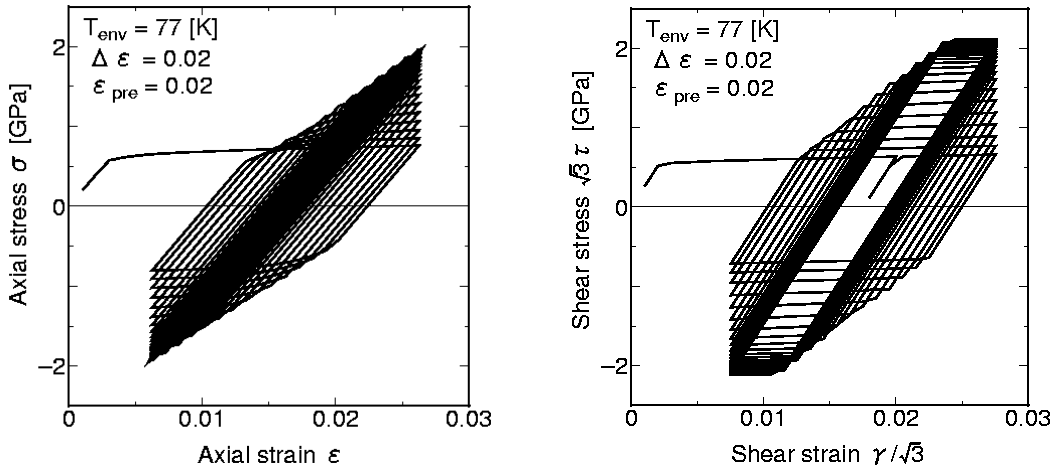

(a) Axial

(b) Shear

Figure 8

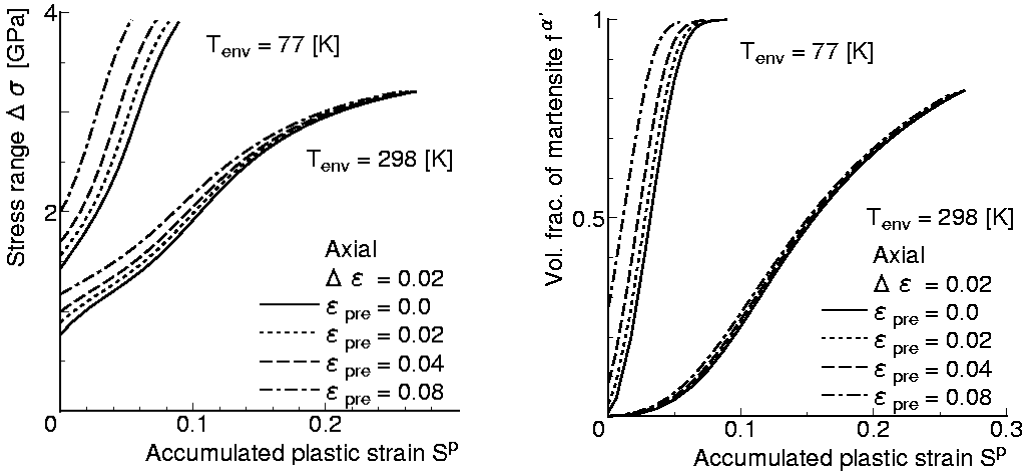
Stress range Δ σ [GPa]
4
2
0
0.1
0.2
Accumulated plastic strain S^p
T_env = 77 [K]
T_env = 298 [K]
Axial
Δ ε = 0.02
ε pre = 0.0
ε pre = 0.02
ε pre = 0.04
ε pre = 0.08
Vol. frac. of martensite f^α'
1
0.5
0
0.1
0.2
0.3
Accumulated plastic strain S^p
T_env = 77 [K]
T_env = 298 [K]
Axial
Δ ε = 0.02
ε pre = 0.0
ε pre = 0.02
ε pre = 0.04
ε pre = 0.08

(a) (b)

Figure 9

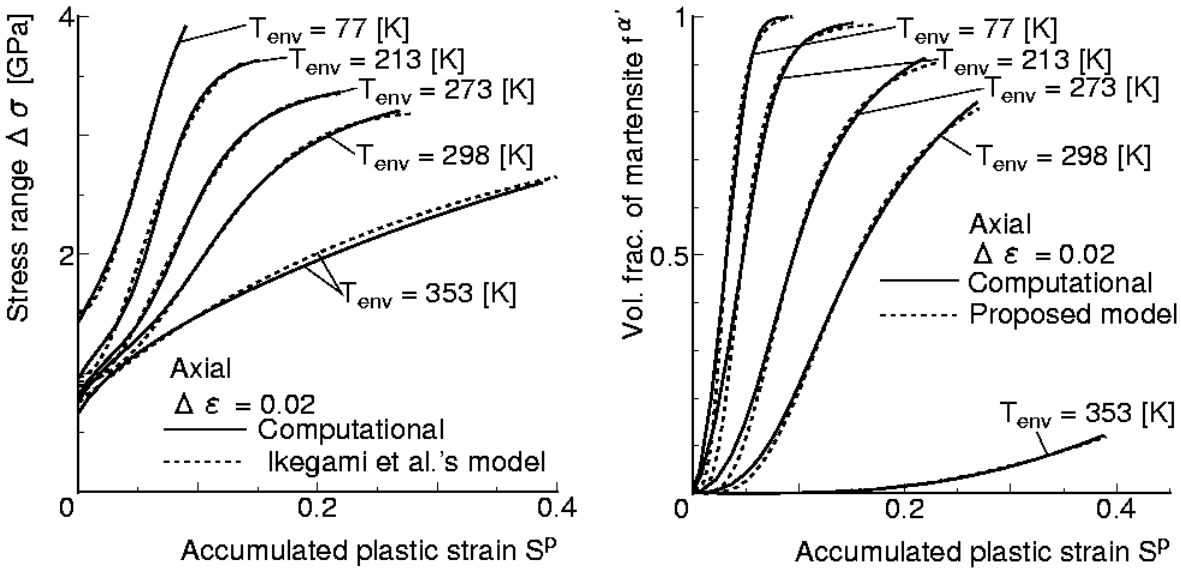
Stress range Δ σ [GPa]
4
2
0
0.2
0.4
Accumulated plastic strain S^p
T_env = 77 [K]
T_env = 213 [K]
T_env = 273 [K]
T_env = 298 [K]
T_env = 353 [K]
Axial
Δ ε = 0.02
Computational
Ikegami et al.'s model
Vol. frac. of martensite f^α'
1
0.5
0
0.2
0.4
Accumulated plastic strain S^p
T_env = 77 [K]
T_env = 213 [K]
T_env = 273 [K]
T_env = 298 [K]
T_env = 353 [K]
Axial
Δ ε = 0.02
Computational
Proposed model

(a) (b)

Figure 10

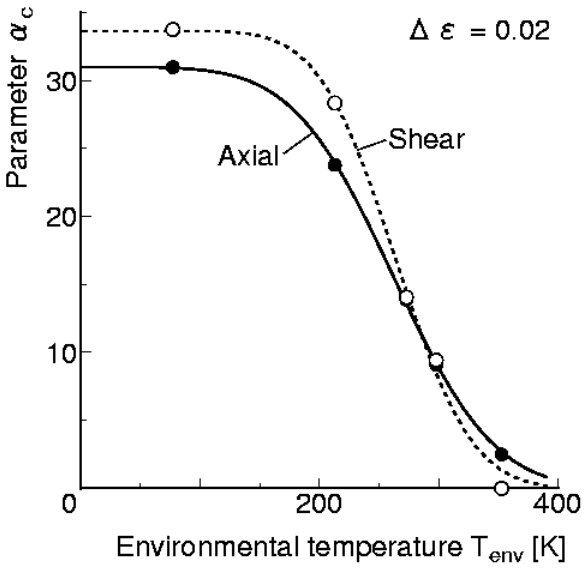

(a) $\alpha_c - T_{env}$

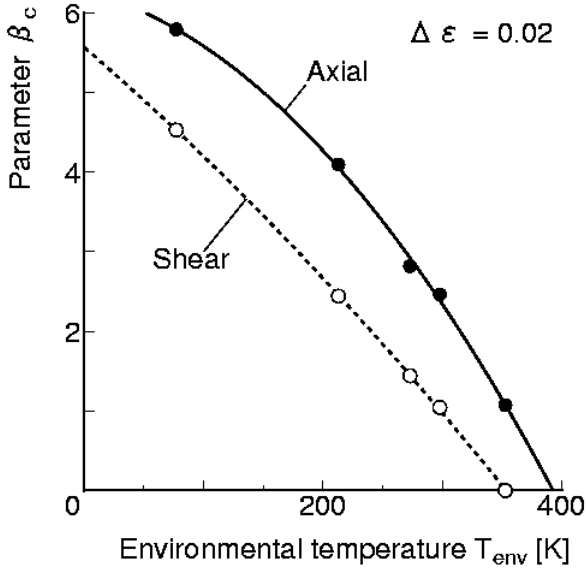

(b) $\beta_c - T_{env}$

Figure 11

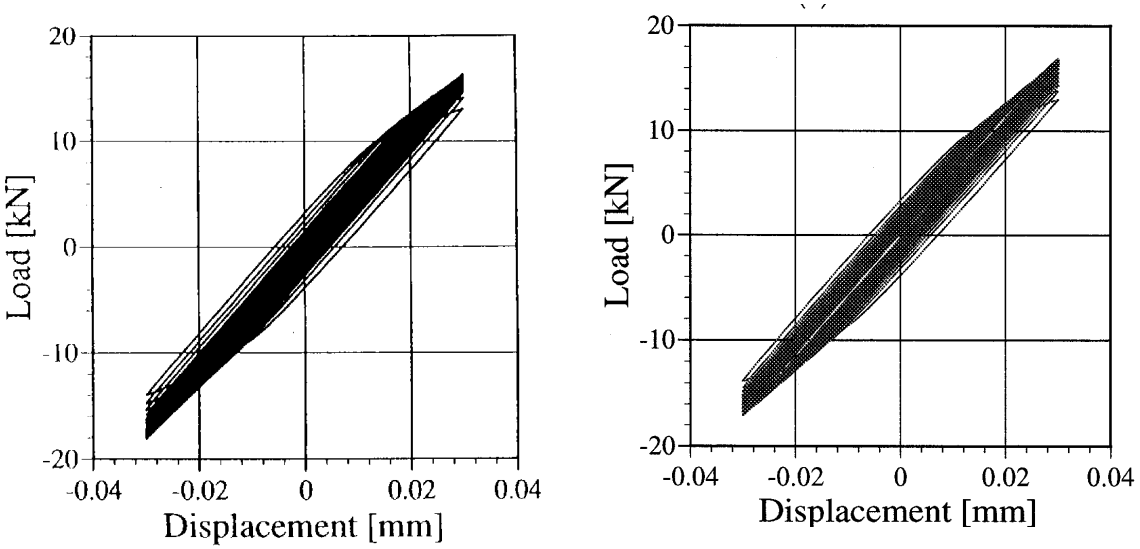

TRIP Steels Austenitic Steel

(a) Load-displacement

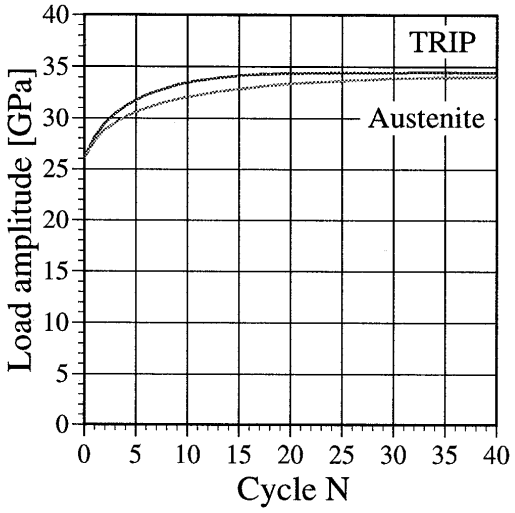

(b) Load amplitude-number of cycles

Figure 12(a)

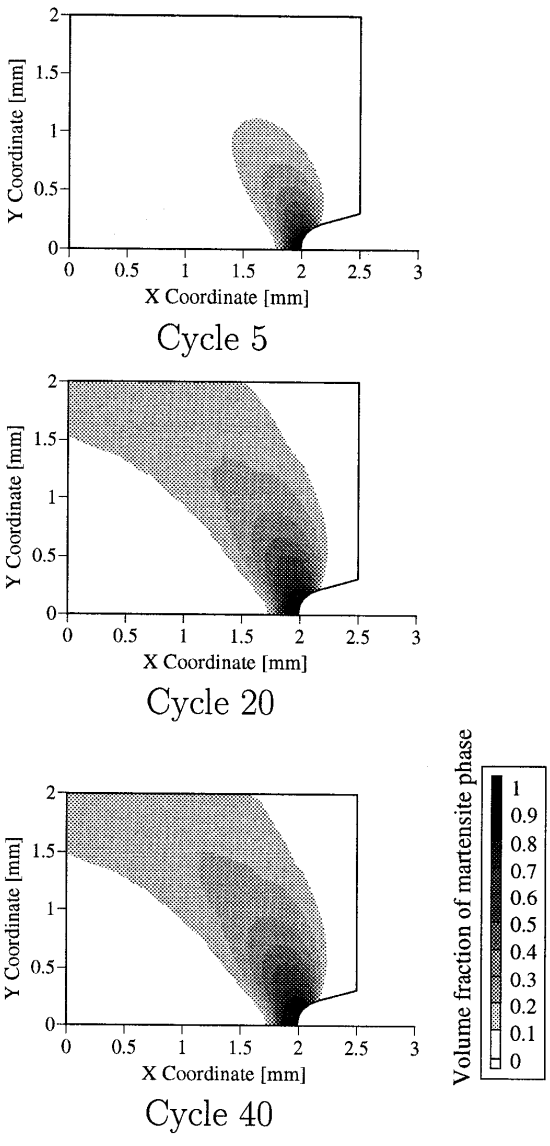
Y Coordinate [mm]
X Coordinate [mm]
Cycle 5
Cycle 20
Cycle 40
Volume fraction of martensite phase
1
0.9
0.8
0.7
0.6
0.5
0.4
0.3
0.2
0.1
0

Figure 12 (b) and (c)

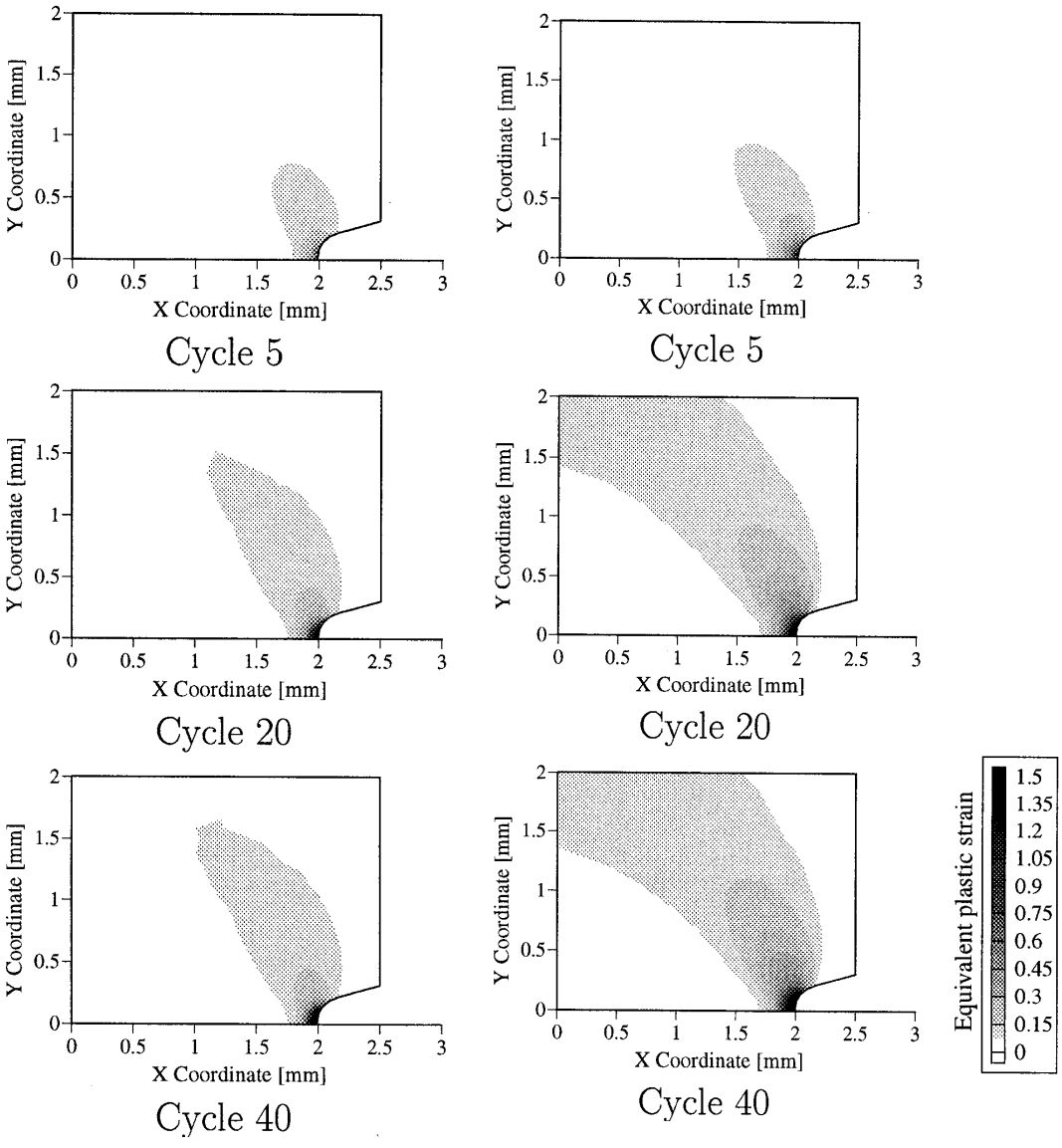

Figure 13

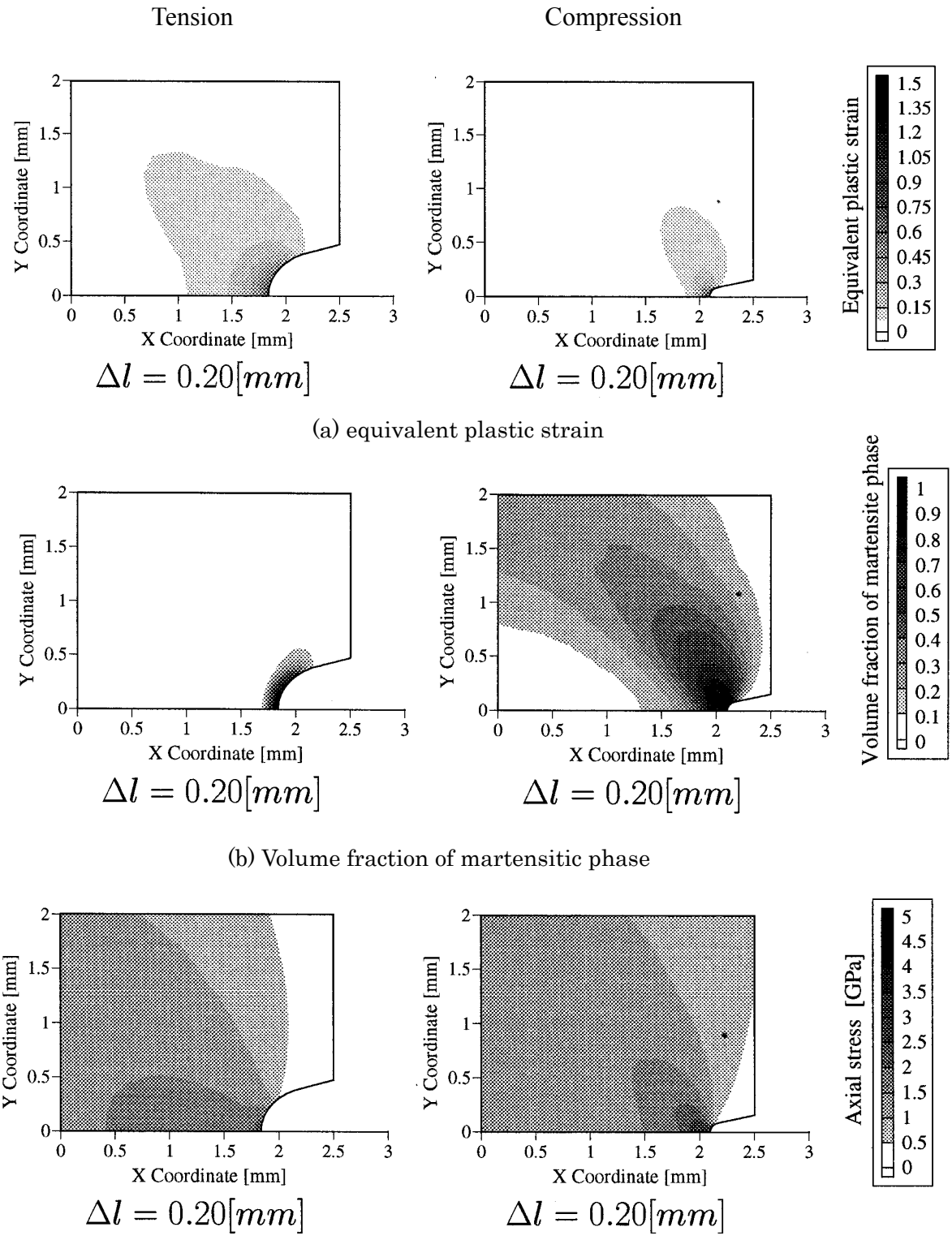

(a) equivalent plastic strain

(b) Volume fraction of martensitic phase

(c) axial stress distribution